

Failure Mechanisms of Stretchable Perovskite Light-Emitting Devices under Monotonic and Cyclic Deformations

Sharafadeen Adeniji, Oluwaseun Oyewole, Richard Koech, Deborah Oyewole, Jaya Cromwell, Ridwan Ahmed, Omolara Oyelade, Dahiru Sanni, Kingsley Orisekeh, Abdulhakeem Bello, and Winston Soboyejo*

This paper presents the results of experimental and analytical studies of the failure mechanisms of stretchable perovskite light-emitting devices (PeLEDs). The multilayered PeLED structures consist of an anodic layer of poly(3,4-ethylenedioxythiophene):polystyrene-sulfonate (PEDOT:PSS), an emissive layer of methylammonium lead bromide (MAPbBr₃), and a eutectic gallium–indium (EGaIn) cathodic layer, which are deposited onto treated polydimethylsiloxane substrates. The intrinsically nonstretchable MAPbBr₃ and PEDOT:PSS are modified with poly(ethylene oxide). The failure mechanisms of the layered stretchable PeLED structures are then investigated under monotonic and cyclic deformations. The optical and scanning electron microscopy images show the deflection and propagation of cracks and wrinkles under applied strains. Cracking of perovskite crystal and debonding of films are also observed with increased cyclic deformation. The effects of the failure mechanisms on the optoelectronic properties of the devices are then studied. The in situ measured transmittance of the PEDOT:PSS ($\approx 75\%$) reduces with increasing uniaxial strain, and then is increased close to its initial value when the strain is released. The turn-on voltage of the device increases with increasing number of cycles between 50 and 1000 cycles at 20% strain level. The fatigue lifetimes of the PeLED structures are used to explain the design of stretchable perovskite devices.

1. Introduction

Light-emitting diodes (LEDs) are semiconductor devices which have been used over the years for decorative, display, medical, and general lighting applications.^[1–6] Conventional LEDs are fabricated on rigid substrates which cannot flex or stretch.^[7–9] However, there is need for next generation of light-emitting devices which can be used for various applications that require stretching, twisting, and bending.^[10,11] These include wearable sensors,^[12,13] stretchable light display,^[14,15] and bioinspired soft robotic systems,^[16,17] where materials that can withstand large strains and geometrical distortions are required.

The flexibility and/or stretchability of thin-film electronic devices depend on the type of polymeric substrates that are used for their fabrication. Gustafsson et al.^[18] have demonstrated fully flexible and mechanically robust LEDs that are based on poly(ethylene terephthalate) (PET) substrates. These devices have been shown to undergo sharp bending without failure,

S. Adeniji, O. Oyewole, R. Koech, D. Oyewole, J. Cromwell, R. Ahmed, W. Soboyejo
 Department of Mechanical Engineering
 Worcester Polytechnic Institute
 100 Institute Road, Worcester, MA 01609, USA
 E-mail: wsoboyejo@wpi.edu

S. Adeniji, O. Oyelade, D. Sanni, A. Bello
 Department of Theoretical and Applied Physics
 African University of Science and Technology
 Km 10 Airport Road, Galadimawa, Abuja, Federal Capital Territory
 900107, Nigeria

S. Adeniji
 Faculty of Natural and Applied Sciences
 Nile University of Nigeria Plot 681, Cadastral Zone C-00, Jabi, Abuja,
 Federal Capital Territory 900001, Nigeria

O. Oyewole, D. Oyewole, R. Ahmed, W. Soboyejo
 Program in Materials Science and Engineering
 Department of Mechanical Engineering
 Worcester Polytechnic Institute
 Worcester, MA 01609, USA

R. Koech, K. Orisekeh, A. Bello
 Department of Materials Science and Engineering
 African University of Science and Technology
 Km 10 Airport Road, Galadimawa, Abuja, Federal Capital Territory
 900107, Nigeria

D. Oyewole
 Physics Advanced Research Center
 Sheda Science and Technology Complex
 Abuja, Federal Capital Territory 904104, Nigeria

W. Soboyejo
 Department of Biomedical Engineering
 Worcester Polytechnic Institute
 60 Prescott Street, Gateway Park Life Sciences and Bioengineering Center,
 Worcester, MA 01609, USA

 The ORCID identification number(s) for the author(s) of this article can be found under <https://doi.org/10.1002/mame.202100435>

DOI: 10.1002/mame.202100435

showing an external quantum efficiency of about 1% as well as a turn-on voltage of 2–3 V. The performance characteristics of these electronic devices have been optimized by tuning materials selection,^[18–20] processing conditions,^[21,22] and design methodologies^[23,24] in a way that improves their mechanical robustness and optoelectronic properties. In addition to PET, some other plastic thin films have also been used as substrate for flexible electronic devices. These include polyimide, poly(ethylene 2,6-naphthalenedicarboxylate), polycarbonate, polyethersulfone, etc.^[10,11,25,26]

The substrates used in the flexible electronic devices have been reported to experience permanent deformation when the applied strain is beyond 5%.^[27] Hence, they are replaced with very compliant elastomers like polydimethylsiloxane (PDMS) and polyurethane when stretching is involved.^[18,28] This motivates several studies that are targeted at investigating the appropriate materials selection, processing conditions, and design techniques that can be deployed to optimize the performance of robust stretchable electronic devices.^[18,25,28–30]

In an effort to improve the mechanical robustness and efficiency of stretchable optoelectronic devices, island–bridge designs^[29–32] have also been used to distribute active components of devices in small, confined regions (which are referred to as island) to allow stretching. These active materials are joined by electrical and/or mechanical interconnectors (bridges), which are narrow and deformable. Hence, when the devices are stretched, the nonstretchable active components are isolated from the strains, which prevents them from being directly stretched in a way that can lead to fracture. This approach has been used extensively to optimize the performance of inorganic semiconductors.^[29,31] However, the stretchability of each device made from this design depends on the interconnectors between the active materials, and the limited space between them gives rise to reduction in their stretchability in the presence of high-level strains. This is a major setback in the implementation of this design for obtaining high spatial resolution for displays.^[33]

Alternatively, prewrinkling/prebuckling technique has been used for fabrication of stretchable organic solar cells^[10,34,35] and LEDs^[33] on PDMS substrates. The technique involves prestretching of the PDMS substrates before depositing intrinsically nonstretchable thin layers of the devices,^[10,33–35] leading to wavy wrinkled/buckled structures after the strains (through the prestretching) have been removed. This structural design gives rise to stretchable devices whose electrical and optical properties are maintained before and after the formation of the wrinkled structures. This methodology improves the resolution of the display without the use of interconnectors which occupy some areas in the previous design.

However, prestretching of substrates for fabricating stretchable LEDs has been observed to produce complex and macroscopic wrinkled structures that are out-of-plane and easily detectable by naked eyes. These out-of-plane wavy structures produce pixels that cause distortion of images in display technology.^[33]

Furthermore, intrinsically stretchable organic light-emitting devices (OLEDs) that operate without wavy wrinkling/buckling structures have also been reported.^[36–38] In these devices, the substrates, the electrodes, and the emitting layers are all stretchable. These produced OLEDs with blue and green colors whose turn-

on voltages are between 4.5 and 6.8 V. Though, this provides new insight into the fabrication of stretchable LEDs, their operational voltages are relatively too high, leading to avoidable high power consumption.^[14] On the other hand, perovskite light-emitting diodes (PeLEDs) have been shown to emit very bright light at relatively low turn-on voltage (i.e., 1.8 V) with very high luminance intensity that are many times greater than their counterparts.^[39–41]

Recently, fully stretchable PeLEDs have been demonstrated^[14,15] by modifying both the emissive perovskite (MAPbBr₃) layer and the anodic poly(3,4-ethylenedioxythiophene):polystyrene-sulfonate (PEDOT:PSS) with poly(ethylene oxide) (PEO) solution. The mixture of MAPbBr₃ and PEO forms a composite structure where the PEO matrix serves as an elastic connector for the nonstretchable MAPbBr₃ crystals. Similar process enables PEDOT:PSS–PEO composite to be stretchable under service condition. The stretchable PeLEDs have been shown to exhibit mechanical robustness which enables them to undergo cyclic loading at 40% strain for up to 100 cycles without deformation.^[14] Similarly, Kim et al.^[15] have also used low concentration of PEO to modify MAPbBr₃ for mechanically robust stretchable PeLEDs that can withstand up to 1000 cycles at 70% tensile strain without significant deformation.

However, the understanding of failure mechanisms of stretchable PeLEDs under monotonic and cyclic loading is essential for the design of reliable and robust structures. In this paper, we report the detailed failure mechanisms and fatigue lifetimes of fully stretchable PeLEDs using film morphology, fatigue stress-life, and Digital Image Correlation (DIC) approach. This has the potential of improving our current understanding of the robustness and reliability of the stretchable PeLEDs. It also provides insights into the processes that control the deformation through crack propagations, delamination, and/or debonding as they occur within the layered structures of PeLEDs.

2. Results and Discussion

To study the effects of the monotonic loading on the failure mechanisms of the films, we deposited the films on stretchable PDMS substrates and stretched to different strain levels. **Figure 1** presents the in situ optical images of the films that were monotonically strained between 0% and 80%. The image of the as-prepared film (**Figure 1a**) shows densely arranged crystals of perovskite within the PEO matrix without cracks or wrinkles. However, the film shows initiation of cracks within PEO matrix as well as wrinkling (**Figure 1b**) under uniaxial strain up to 20%. The wrinkles are formed parallel to the direction of the applied strains, while cracks are in perpendicular directions to the applied strain. The wrinkles and cracks increase significantly as the strain increases to 40% and 80% (**Figure 1c,d**). Upon release of the strain, the wrinkles and cracks are no more visible, and the surface appears almost like that of the as-prepared film (as shown in **Figure 1e**). These imply that the structural integrity of the films is maintained even with the presence of applied strain (between 0% and 80%). The strain effects are mainly on the stretchable PEO matrix which is evident in the crack initiation. Similar cracking phenomenon has been reported for stretchable perovskite films.^[14,15]

We observed more closely the failure mechanisms of the films using scanning electron microscope (SEM). The SEM images of

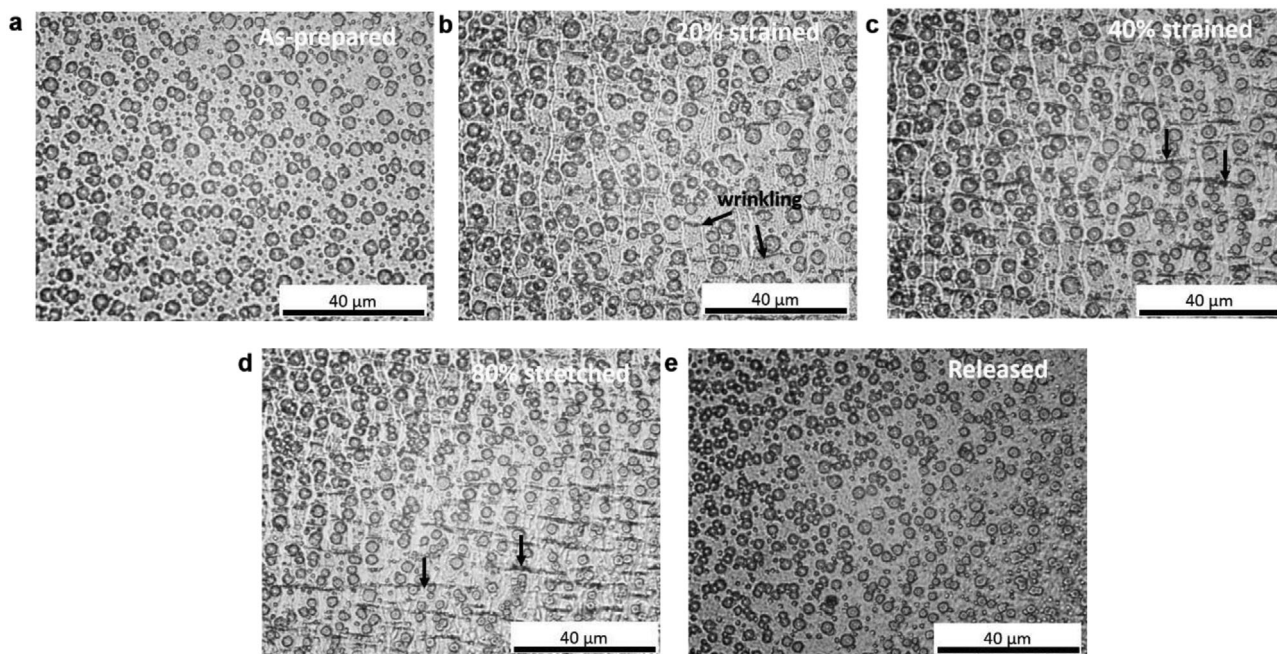


Figure 1. Optical images of PeLED films undergoing monotonic loading: a) as-prepared film, b) film under 20% strain, c) film under 40% strain, d) film under 80% strain, e) after release from strain.

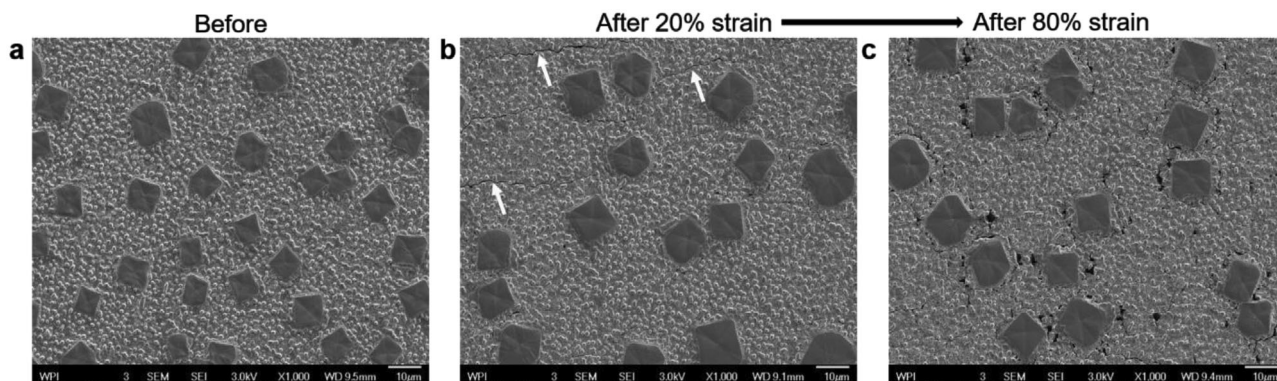


Figure 2. SEM images of PeLED films under monotonic loading: a) as-prepared film, b) film after release from 20% strain, c) film after release from 80% strain. The white arrows indicate the points of crack initiation.

the as-prepared and strained films are presented in **Figure 2a–c**. As observed in the optical image (Figure 1a), the SEM image (Figure 2a) of the as-prepared PeLED film shows dense arrangement of perovskite crystals within the PEO matrix with no evidence of cracks. However, the cracks are present in the SEM images of the strained films. The prevalence and depth of the cracks increase with higher strains (Figure 2b,c). The absence of cracks within the perovskite crystals is an indication that the crystals are isolated during stretching as the effects of the strain are mainly observed on the surface of the PEO. The perovskite crystals are however further apart and less densely arranged on the strained films (Figure 2b,c).

Now that catastrophically cracking is evident within the PEO matrix (Figure 2c) at 80% strain, further study on evolution of lo-

calized strains within the stretchable PeLED structures at lower applied strains (0–40%) was done to provide insights into failure. We took high-resolution videos of the films during monotonic loading and analyzed the strains using a Digital Imaging Correlation (DIC) technique. **Figure 3** presents the strain–time curves of the PeLED structures and their strain distributions during the monotonic loading. The strain–time curves (Figure 3a,b) show that the PeLEDs films experienced both tension and compression within the estimated transverse (Figure 3a), shear (Figure 3b), and axial (Figure 3c) strains. The range of strains along axial directions (Figure 3c) is higher compared to transverse and shear strains, indicating possible cracking as the monotonic loads are being applied. The blue and red colors on the strain distribution images (Figure 3d–i) indicate regions with compression and

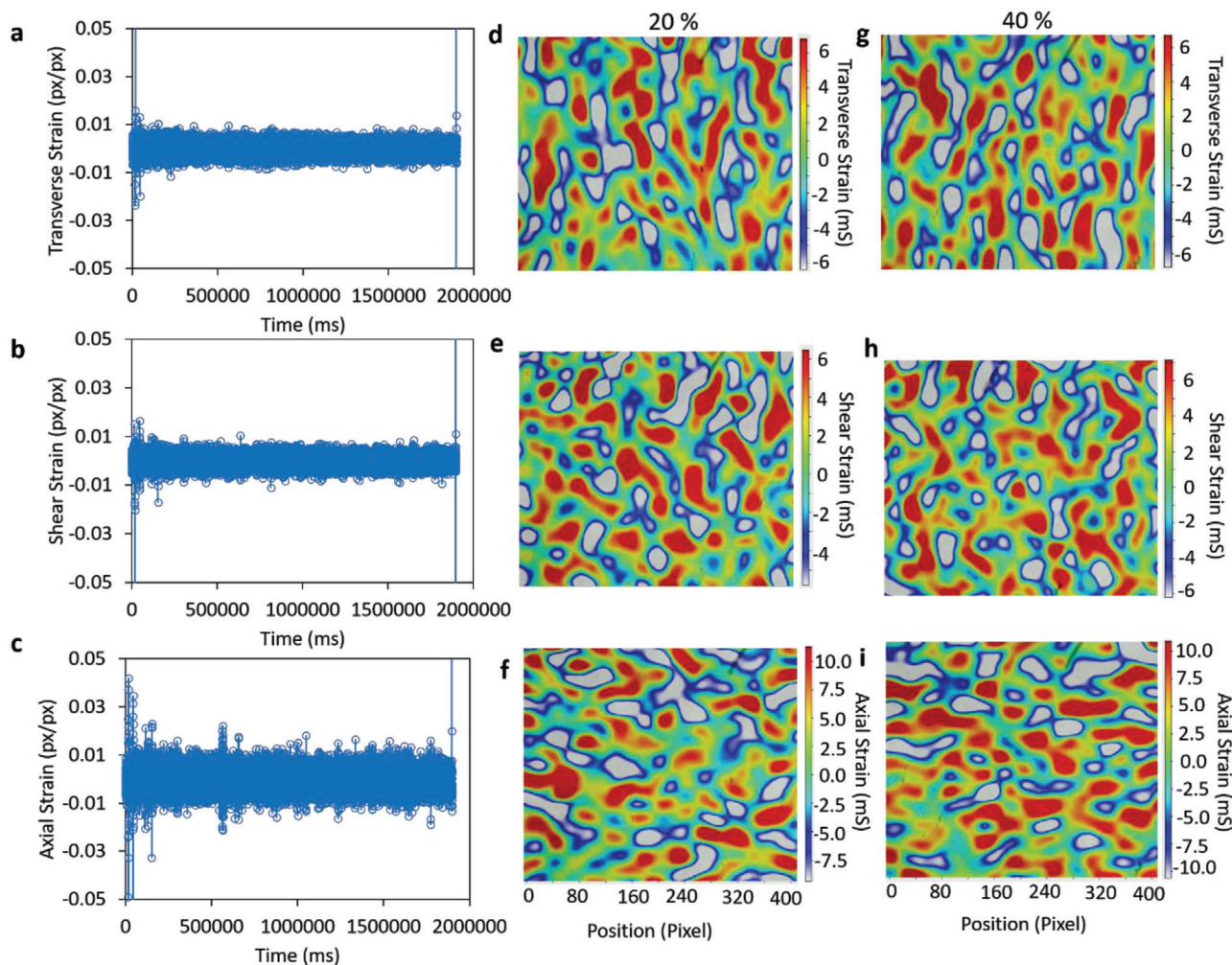


Figure 3. Evolution of strain state during monotonic loading: a–c) strain–time curves for transverse, shear, and axial strains, d–f) strain distributions at 20% monotonic strain for transverse, shear, and axial strains, g–i) strain distributions at 40% monotonic strain for transverse, shear, and axial strains.

tension, respectively. The regions of tension are described as regions with tendency of cracking within the PEO matrix (as shown in Figure 2b,c) at higher strains while the compression regions are dominated by wrinkling formation (as shown in Figure 1b–d) within the stretchable PeLEDs films. We also see an increase in the strain distribution in transverse (Figure 3d,g), shear (Figure 3e,h), and axial (Figure 3f,i) directions, as the applied monotonic strain increases.

We give insights into the reliability of the structures of stretchable PeLEDs by carrying out load-controlled cyclic deformation tests on the PeLED films to evaluate their fatigue lifetimes. For each of the applied loads, the strain range was estimated from the sinusoidal strain–lifetime plot (Figure 4a). Figure 4b presents the plot of the total strain ranges as a function of the number of cycles. The strain range of the bare PDMS substrate is found to be $\approx 50\%$ at a maximum load of 5 N for over 1000 repeated stretching. The same 5 N load was applied on the coated PDMS substrate and subjected to over 1000 repeated cycles. Then, the strain range reduces to $\approx 38\%$. When the maximum load is reduced to 3.5 N on the coated PDMS, the strain range reduces to about 34%. This

trend continues as the strain ranges for 2.5 and 1.5 N loads reduced to about 18% and 2%, respectively. The strain ranges are observed to decrease as the magnitude of the load decreases from 5 to 1.5 N (Figure 4b). The strain ranges also increase after undergoing certain number of cycles. In the case of the 5 and 3.5 N loads on coated PDMS substrates accompanied with cyclic loadings, the deformation penetrates through the coated films and get to the PDMS substrate. Hence, the strain ranges later behave almost like that of the bare PDMS substrate. The loads in 2.5 and 1.5 N, on the other hands, are not enough to penetrate the film like the higher loads. Hence, their strain ranges are completely lower than that of the bare PDMS throughout the testing period. This trend is consistent with the earlier work reported by Oyewole et al.^[34]

To provide more insights into the fatigue behavior of the stretchable PeLED films, we incorporated the number of cycles to failure and the strain range into Coffin–Manson relation (Equation (1)). The log–log plot of the total strain range ($\Delta\epsilon/2$) against the total number of load reversals to failure ($2N_f$) is presented in Figure 4c for the stretchable PeLED films. The

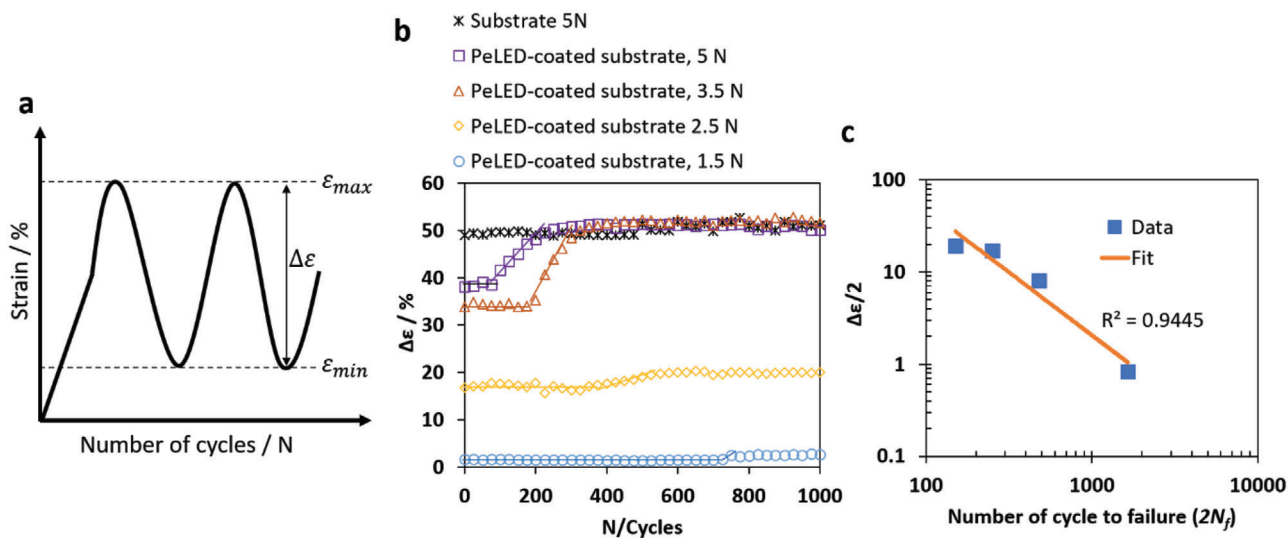


Figure 4. Fatigue tests on the device: a) Schematic of cyclic loading on the PeLED films. b) Plot of the total strain range–number of cycles. c) Log–log plot of strain range–number of load reversal to failure.

number of load reversal to failure corresponds to the number of cycles at the initial strain range before the strain range increases

$$(\Delta\epsilon/2) = \epsilon'_f (2N_f)^c \quad (1)$$

where $(\Delta\epsilon/2)$ is the strain amplitude, ϵ'_f is the fatigue ductility coefficient, N_f is the number of cycles to failure, and c is the fatigue ductility exponent. The value of the estimated fatigue ductility exponent of the PeLED is ≈ -0.04 . This value indicates that fatigue ductility of fully stretchable PeLEDs is very high compared to prewrinkled stretchable organic structures^[34] and stretchable metallic thin film (with exponent of ≈ -0.4).^[42] It is important to note that materials with higher ductility exponent can accommodate higher repeated strains before failure. In the case of stretchable PeLEDs, the incorporation of PEO into perovskite materials has engineered its robustness and stretchability.

To study the effects of cyclic loading on the failure mechanisms of the PeLED films, the images of the cyclically deformed films were observed under SEM at different maximum strains (20%, 40%, and 80%). Cracking failure is dominant in all the observed images (Figure 5a–i), but the cracks increase with increasing applied strain as well as the number of cycles. The cracks at low strain and low number of cycles are deflecting and/or propagating through the PEO matrix only. The perovskite crystals are isolated from the stretching as cracks can be observed within the PEO matrix. These cracks increased with increasing number cycles (Figure 5c, f) and strain (Figure 5g–i). In addition to the cracks within the PEO, some cracks are also observed within the boundaries of clustered perovskite crystals at higher number of cycles (Figure 5c). Most importantly, delamination and/or debonding of the film from the substrate was observed at higher strain of 80% after 2000 cycles (Figure 5i). Detailed SEM images that show the failure mechanisms of the PeLEDs films are presented in detail in Figures S1–S3 (Supporting Information) for different maximum strains, 20%, 40%, and 80%, respectively.

We also studied the effects of monotonic and cyclic deformation on optical properties of the stretchable PeLED films. The

in situ optical transmittance of the PEDOT:PSS–PEO film (anodic layer) was measured under monotonic loading. Figure 6a presents the results of the transmittance of the stretchable PEDOT:PSS films. The as-prepared stretchable PEDOT:PSS sample gives a transmittance of $\approx 75\%$ at about 535 nm. This value reduces continuously as the monotonic strains increased between 20% and 80% are applied. The result shows that though the transmittance reduces as the strain increases, the film is still capable of transmitting light as shown (Figure 6a). It is also important to note that the applied strains tend to reduce film thickness, which can also cause the decrease in the film transmittance. The transmittance was also observed when the strain was removed, and its peak was close to that of the as-prepared film. This also shows that the PEDOT:PSS crystals are not directly affected by the stretching of the films, but the PEO matrix has been continuously stretched. The reduction in the transmittance of the stretchable PEDOT:PSS film is associated with effective effects of the observed cracking and wrinkling (Figure 1). The absorbance and photoluminescence (PL) spectra of the emitting layer of the stretchable PeLEDs (MAPbBr₃) are also investigated under cyclic loadings. Figure 6b shows the absorbance of the as-prepared and cyclically deformed films. The films were strained up to 40% and went through 400 and 1000 repetitive stretching. The peaks reduce as the number of cycles increases. The same trend is observed in the PL spectra (Figure 6c) that was carried out on the stretchable PeLED layer. The peaks at about 535 nm decrease as the number of cycles increases (Figure 6c). The reduction in the absorbance and PL peaks after stretching can be attributed to the reduction in the number of perovskite crystals on each region of the films, during and after stretching. This can be observed in Figure 5d–f, as the densely arranged crystals in the as-prepared films become further apart when strained and/or cycled.

To demonstrate the effects of cyclic deformation on the performance characteristics of stretchable PeLEDs, we obtained current–voltage (I – V) curves of the fabricated stretchable PeLED devices and estimated the turn-on voltages after different

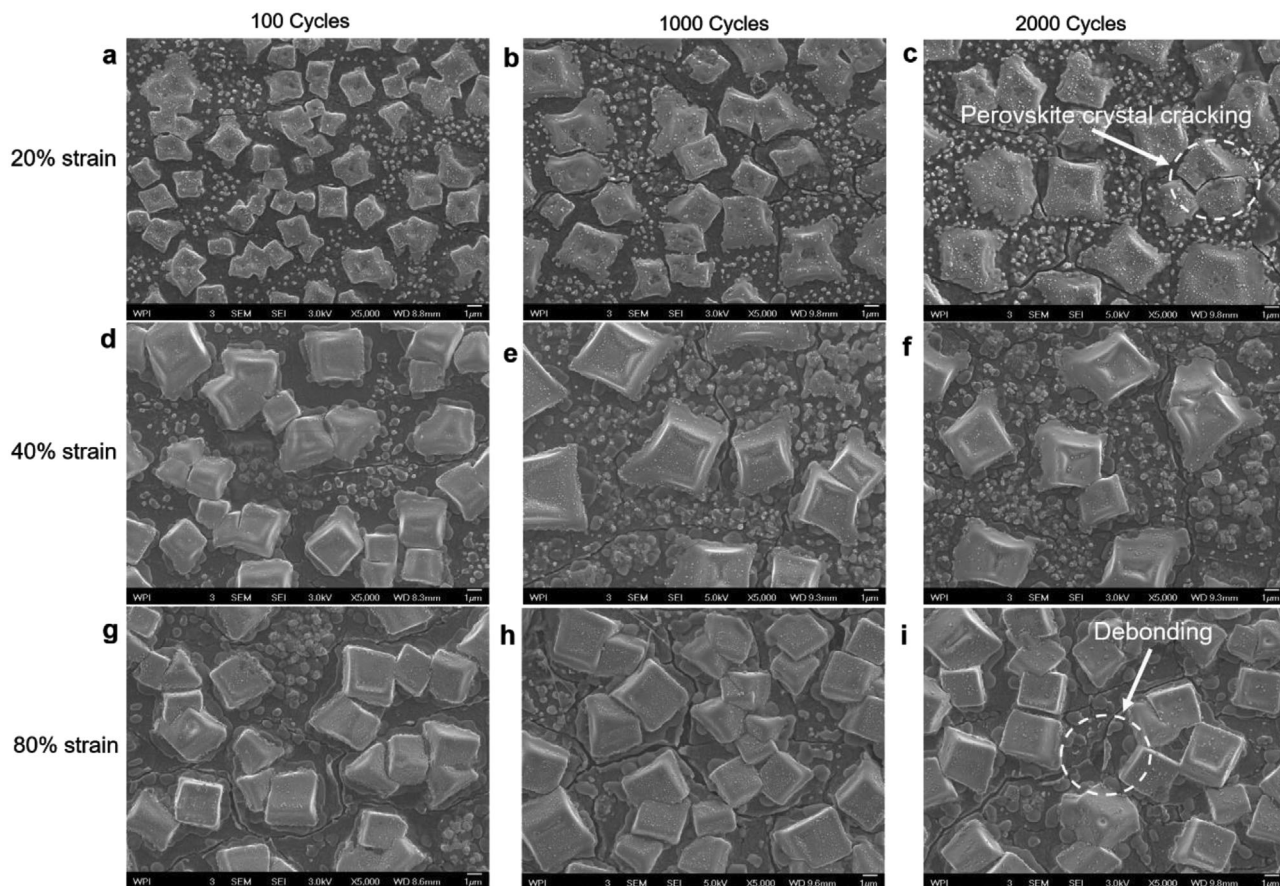


Figure 5. SEM images of PeLED films after cyclic loadings: a–c) PeLED films with 20% strain after 100, 1000, and 2000 cycles, respectively, d–f) PeLED films with 40% strain after 100, 1000, and 2000 cycles, respectively, g–i) PeLED films with 80% strain after 100, 1000, and 2000 cycles, respectively.

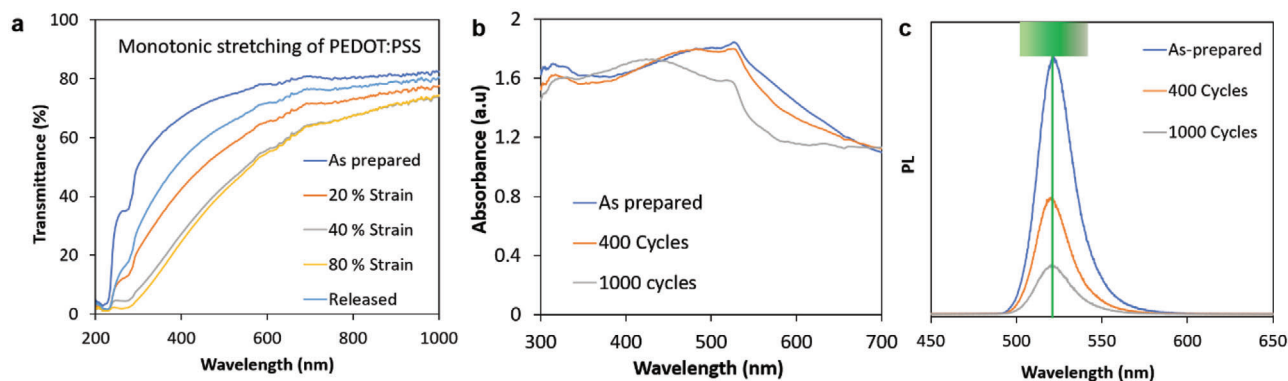


Figure 6. a) Transmittance of the anodic layer under monotonic loadings. b) Absorbance of the emitting layer under cyclic loadings. c) PL spectrum of the emitting layer under cyclic loading.

number of cycles at a maximum strain of 20%. **Figure 7a** presents the I – V curves of as-prepared and deformed stretchable PeLEDs. The turn-on voltages of the devices are presented in **Figure 7b** for different number of cycles. Although the devices keep working after 1000 cycles, their turn-on voltages increase with increasing number of cycles. The increase in the turn-on voltage is attributed to the observed cracking and debonding of the films. The reduction in the number of perovskite crystals

at a given region, due to plastic deformation of PEO matrix at higher cycles, can also make the devices to turn-on at higher bias voltage. The reduced electrical performance of the stretchable PeLEDs is also attributed to increase in resistance of the anodic PEDOT:PSS (**Figure 8a**) due to cracking (**Figure 8b,c**). There is also an evidence of propagation of cracks from top to bottom of the perovskite/PEDOT:PSS/PDMS layered structure (**Figure 8d,e**) that can reduce the device performance.

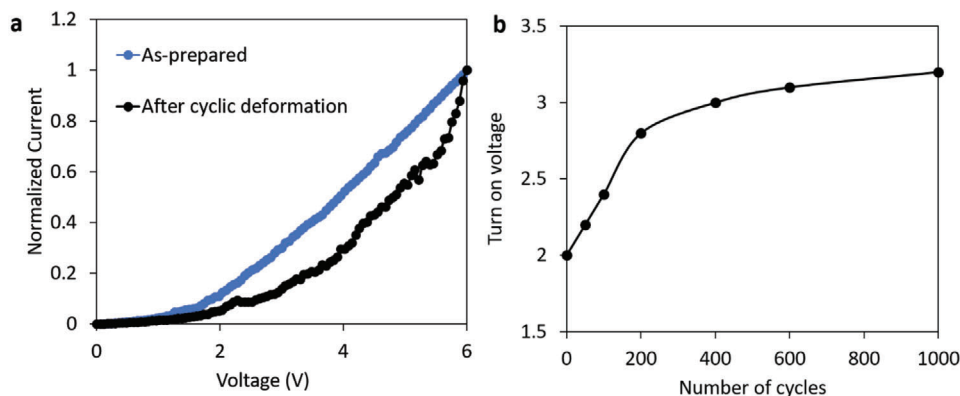


Figure 7. Effects of cyclic deformation on performance characteristic of stretchable PeLEDs: a) *I*-*V* curves and b) estimated turn-on voltage versus number of cycles for 20% strain.

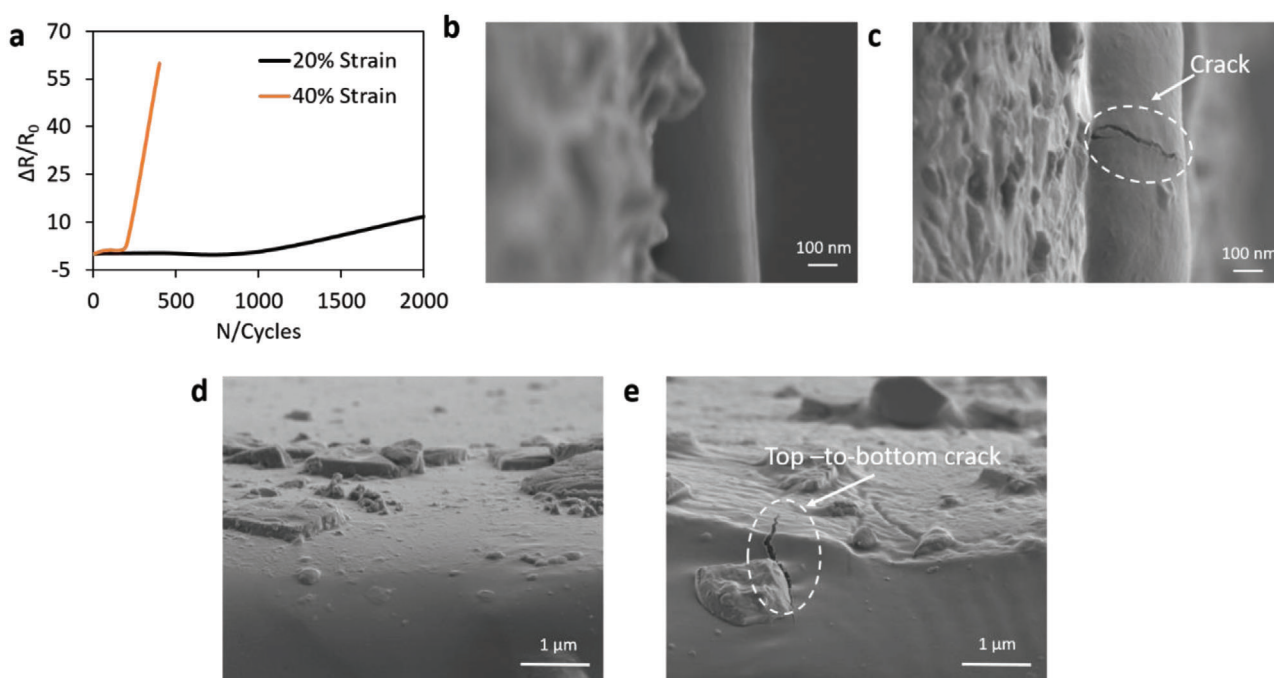


Figure 8. a) Resistance of cyclically deformed PEDOT:PSS film on PDMS at 20% and 40%, b,c) cross-sectional SEM images of PEDOT:PSS a) before and b) after 1000 cyclic deformation at 40% strain, and d,e) cross-sectional SEM images of layered perovskite on PEDOT:PSS/PDMS a) before and b) after 1000 cyclic deformation at 40% strain.

3. Conclusion

In conclusion, we present the failure mechanisms of stretchable perovskite light-emitting devices whose emissive (MAPbBr₃) and anodic (PEDOT:PSS) materials are modified with PEO to enhance the stretchability of the entire devices. The results show the effects of monotonic and cyclic loading on the failure of the PeLEDs. The deformation is associated with the initiation and propagation of cracks which increase as the uniaxial strain and number of cycles increase. However, the cracks are mainly isolated within the PEO matrix which serves as an elastic medium for the intrinsically nonstretchable MAPbBr₃ and PEDOT:PSS.

The consequence of this deformation is examined on the optical transmittance of PEDOT:PSS-PEO (anodic layer), the absorbance of the MAPbBr₃-PEO (emissive layer), and the current-voltage characteristics of the stretchable PeLEDs.

The optical properties of the PeLEDs are found to reduce as the devices undergo monotonic and cyclic loading. The optical transmittance of the anodic layer and the absorbance of the emissive layer reduce with increasing strain and number of cycles, respectively. The stretchable PeLEDs are shown to be mechanically robust as they can withstand cyclic deformation with up to 80% strain without significant deformation on the perovskite crystals. The samples exhibit their optical properties even at 80% strain

with 1000 repetitive stretching. Beyond this threshold, specifically with 2000 cycles at 80% strain, the films delaminate and/or debond from the PDMS substrates.

The current–voltage characteristics of the PeLEDs are also influenced by the monotonic and cyclic loadings. At 20% strain, the turn-on voltages of the PeLEDs are found to increase as the number of cycles increase. The influence of the deformation on the optoelectronic properties of the PeLEDs are associated with the perovskite crystals which become farther apart within a given region as the samples undergo monotonic and/or cyclic loading.

The fatigue lifetimes of the PeLEDs are also predicted for the multilayer structures by using a Coffin–Manson relation. Essentially, this work provides more insights into the opportunities that are associated with perovskite materials as promising materials for stretchable optoelectronic devices that can withstand geometric distortion at higher strain and cycles.

4. Experimental Section

Materials: Dimethyl sulfoxide (DMSO, anhydrous, $\geq 99.9\%$), *N,N*-dimethylformamide (DMF, anhydrous, 99.8%), lead (II) bromide (PbBr_2 , $\geq 99.999\%$), methyl ammonium bromide (MABr, $\geq 99\%$), PEDOT:PSS (PEDOT:PSS, H. C. Starck, Newton, MA, USA), poly(ethylene) (PEO) ($M_w = 5\,000\,000$), and gallium–Indium eutectic ($\geq 99.99\%$ trace metals) were purchased from Sigma-Aldrich (USA). Triton X-100 was purchased from EMD Millipore Corporation (USA) and Sylgard 184 silicone elastomer base and its curing agent were purchased from Dow Corning Corp.

Fabrication of Stretchable PeLEDs: The PDMS substrates were fabricated by mixing the Sylgard 184 silicone elastomer (Sylgard 184, Dow Corning Corp.) base and its curing agent in weight ratio of 10:1 wt%. The mixture was mixed thoroughly before pouring into a cuboid-shaped mold made from shinning silicon wafer which has a depth of about 0.5 mm. The mixture was then degassed in a vacuum oven with a pressure of 25 kPa to remove trapped bubbles. This was then followed by curing of the PDMS at 70 °C for 2 h. The PDMS was cut into smaller pieces (with dimensions 50 mm \times 5 mm \times 0.5 mm) before placing them on cleaned glass slides. It is important to note here that the surface of the PDMS substrate that was cured against the shinning silicon wafer faced up. The PDMS substrates were treated with oxygen plasma (HARRICK PLASMA, PDC -100 -HP, NY, USA) for 2 min to remove organic contamination, increase surface wettability, and render them hydrophilic. A composite from the mixture of aqueous PEDOT:PSS and PEO solution was used as stretchable anode. This was prepared by mixing PEDOT:PSS, DMSO, and Triton X-100 in volume ratio of 93:5:2, respectively. The DMSO solution was added to improve the conductivity of PEDOT:PSS while TritonX-100 improves its wettability on PDMS.^[34] Also, the PEO solution was prepared by dissolving PEO in DMF to give a concentration of 10 mg mL⁻¹. Then, the PEDOT:PSS–PEO composite was obtained by using 33 wt% PEO as optimized by Bade et al.^[14] The mixture was stirred for 2 h at 1500 rpm to ensure homogenous mixture. This produced stretchable PEDOT:PSS solution that was spin-coated on the treated PDMS substrates at 2000 rpm for 30 s. The resulting films were annealed at 110 °C for 10 min on a hot plate.

The stretchability of the emitting material (MAPbBr_3) was also enhanced by the addition of PEO. The precursor solution for emitting layer was prepared by dissolving PbBr_2 and $\text{CH}_3\text{NH}_3\text{Br}$ (in molar ratio of 1:1.5, respectively) in anhydrous DMSO to obtain MAPbBr_3 solution with concentration of 500 mg mL⁻¹. The solution was stirred for 30 min at 70 °C and it was filtered using a 0.45 μm mesh. The PEO solution was then mixed with the filtered MAPbBr_3 solution in the ratio of 1:39 wt%,^[15] respectively, to form MAPbBr_3 –PEO composite emitter that could be stretched. The mixture was also stirred at 70 °C for 30 min and was spin-coated on the PEDOT:PSS–PEO/PDMS substrates at 1500 rpm for 60 s. This was followed by thermal annealing at 80 °C for 5 min.

Finally, a drop of eutectic gallium–indium eutectic (EuGal) was dispensed on the perovskite film through a syringe. The schematics of the

device fabrication process are presented in Figure S4 in the Supporting Information.

Monotonic and Cyclic Loading Experiments: The samples of the stretchable multilayered films (MAPbBr_3 –PEO/PEDOT:PSS–PEO/PDMS films) of dimension 5 mm \times 50 mm \times 0.5 mm were subjected to uniaxial tensile tests using Instron machine (Instron 8872, Instron, Norwood, MA, USA). The Instron machine was instrumented with a very sensitive calibrated 10 N load cell (10 N Load cell, Instron Norwood, MA, USA). The cross head of the machine was operated at a speed of 1 mm min⁻¹ to strain the samples to different strain levels of 20%, 40%, and 80%. The local displacements in the samples were captured and recorded using high-resolution digital microscope, which were further analyzed using a DIC technique.

The fatigue tests were carried out on the bare PDMS substrates and the coated PDMS films using Servohydraulic Instron machine (Instron 8872, Instron, Norwood, MA, USA) which was instrumented with a 10 N load cell. The cyclic loading was performed under load control between 1.5 and 5.0 N. The detailed procedures for the cyclic loading were similar to previous steps reported by Oyewole et al.^[34] and Kraft et al.^[42]

Characterization: The transmittance of anodic stretchable (PEDOT:PSS–PEO) was measured in situ under monotonic loading using a UV-vis–NIR spectrometer (Avantes, BV, USA). The absorbance spectra of the stretchable emitting layer were also measured after cyclic loading at a maximum strain of 40%. These were obtained for the as-prepared samples and those deformed at 40% strain over 400 and 1000 cycles.

The PL spectrum measurements were obtained for both the as-prepared and cyclically loaded samples, using Horiba MicroOS microscope optical spectrometer. The system used a Horiba iHR550 spectrometer, a luminescence microscope with a 50x Edmund Optics Plan Apo NIR Mitutoyo objective, and a Horiba Synapse EM CCD camera. A single photon counter module (SPD-OEM-VIS, Aurer technology) and an acquisition software interface were used to obtain the PL spectrum measurements for the samples.

In situ optical images of the stretchable films were obtained under monotonic loading at 20%, 40%, and 80% strains using an OMAX optical microscope (OMAX, 40–3000 \times 18MP, Gyeonggi-do, South Korea). The images of the as-prepared and the released films were also taken. Moreover, the images of samples that were cyclically loaded were obtained using an SEM (JEOL JSM-700F, Hollingsworth & Vose, MA, USA). The current density–voltage (*I*–*V*) curves were also measured using a Keithley 2400 source meter unit (SMU) system (Keithley, Tektronix, Newark, NJ, USA).

Supporting Information

Supporting Information is available from the Wiley Online Library or from the author.

Acknowledgements

The authors are grateful to the Worcester Polytechnic Institute for financial support. The authors also thank the Pan African Materials Institute (PAMI), one of the World Bank African Centers of Excellence Program at the African University of Science and Technology (AUST), for their financial support (grant no. P126974).

Conflict of Interest

The authors declare no conflict of interest.

Data Availability Statement

Research data are not shared.

Keywords

cracking, failure mechanisms, monotonic and cyclic deformations, perovskite-PEO, stretchable perovskite light-emitting diodes

Received: June 15, 2021

Revised: August 3, 2021

Published online:

-
- [1] E. Boonekamp, *WO/2010/070557*, **2011**.
- [2] W.-J. Tseng, *US 7,422,489 B1*, **2008**.
- [3] H.-W. Chen, J.-H. Lee, B.-Y. Lin, S. Chen, S.-T. Wu, *Light: Sci. Appl.* **2018**, *7*, 17168.
- [4] S. Kim, H. Kwon, S. Lee, H. Shim, Y. Chun, W. Choi, J. Kwack, D. Han, M. Song, S. Kim, *Adv. Mater.* **2011**, *23*, 3511.
- [5] N. G. Yeh, C.-H. Wu, T. C. Cheng, *Renewable Sustainable Energy Rev.* **2010**, *14*, 2161.
- [6] T. Elze, C. Taylor, P. J. Bex, *Med. Phys.* **2013**, *40*, 092701.
- [7] J. Asare, S. A. Adeniji, O. K. Oyewole, B. Agyei-Tuffour, J. Du, E. Arthur, A. A. Fashina, M. G. Zebaze Kana, W. O. Soboyejo, *AIP Adv.* **2016**, *6*, 065125.
- [8] O. V. Oyelade, O. K. Oyewole, D. O. Oyewole, S. A. Adeniji, R. Ichwani, D. M. Sanni, W. O. Soboyejo, *Sci. Rep.* **2020**, *10*, 7183.
- [9] F. Guo, A. Karl, Q. Xue, K. C. Tam, K. Forberich, C. J. Brabec, *Light: Sci. Appl.* **2017**, *6*, e17094.
- [10] D. J. Lipomi, Z. Bao, *Energy Environ. Sci.* **2011**, *4*, 3314.
- [11] S. J. Benight, C. Wang, J. B. H. Tok, Z. Bao, *Prog. Polym. Sci.* **2013**, *38*, 1961.
- [12] J. H. Koo, S. Jeong, H. J. Shim, D. Son, J. Kim, D. C. Kim, S. Choi, J.-I. Hong, D.-H. Kim, *ACS Nano* **2017**, *11*, 10032.
- [13] H. E. Lee, D. Lee, T.-I. Lee, J. H. Shin, G.-M. Choi, C. Kim, S. H. Lee, J. H. Lee, Y. H. Kim, S.-M. Kang, *Nano Energy* **2019**, *55*, 454.
- [14] S. G. R. Bade, X. Shan, P. T. Hoang, J. Li, T. Geske, L. Cai, Q. Pei, C. Wang, Z. Yu, *Adv. Mater.* **2017**, *29*, 1607053.
- [15] H. M. Kim, Y. C. Kim, H. J. An, J.-M. Myoung, *J. Alloys Compd.* **2020**, *819*, 153360.
- [16] J. Rossiter, *Nat. Mater.* **2020**, *19*, 134.
- [17] F. Hartmann, M. Baumgartner, M. Kaltenbrunner, *Adv. Mater.* **2020**, *33*, 2004413.
- [18] G. Gustafsson, Y. Cao, G. M. Treacy, F. Klavetter, N. Colaneri, A. J. Heeger, *Nature* **1992**, *357*, 477.
- [19] L. Zhou, H.-Y. Xiang, S. Shen, Y.-Q. Li, J.-D. Chen, H.-J. Xie, I. A. Goldthorpe, L.-S. Chen, S.-T. Lee, J.-X. Tang, *ACS Nano* **2014**, *8*, 12796.
- [20] J.-W. Kang, W.-I. Jeong, J.-J. Kim, H.-K. Kim, D.-G. Kim, G.-H. Lee, *Electrochem. Solid State Lett.* **2007**, *10*, J75.
- [21] S. Hou, M. K. Gangishetty, Q. Quan, D. N. Congreve, *Joule* **2018**, *2*, 2421.
- [22] Q. Dong, L. Lei, J. Mendes, F. So, *J. Phys. Mater.* **2020**, *3*, 012002.
- [23] S. Y. Lee, S.-H. Kim, Y. S. Nam, J. C. Yu, S. Lee, D. Bin Kim, E. D. Jung, J.-H. Woo, S. Ahn, S. Lee, *Nano Lett.* **2019**, *19*, 971.
- [24] D. Yu, O. K. Oyewole, D. Kwabi, T. Tong, V. C. Anye, J. Asare, E. Rwenyagila, A. Fashina, O. Akogwu, J. Du, *J. Appl. Phys.* **2014**, *116*, 074506.
- [25] G. Fortunato, A. Pecora, L. Maiolo, *Mater. Sci. Semicond. Process.* **2012**, *15*, 627.
- [26] W. A. MacDonald, M. K. Looney, D. MacKerron, R. Eveson, R. Adam, K. Hashimoto, K. Rakos, *J. Soc. Inf. Disp.* **2007**, *15*, 1075.
- [27] A. Pegoretti, A. Guardini, C. Migliaresi, T. Ricco, *J. Appl. Polym. Sci.* **2000**, *78*, 1664.
- [28] M. M. Tavakoli, Q. Lin, S.-F. Leung, G. C. Lui, H. Lu, L. Li, B. Xiang, Z. Fan, *Nanoscale* **2016**, *8*, 4276.
- [29] J. Lee, J. Wu, M. Shi, J. Yoon, S.-I. Park, M. Li, Z. Liu, Y. Huang, J. A. Rogers, *Adv. Mater.* **2011**, *23*, 986.
- [30] Y. Zhang, H. Fu, Y. Su, S. Xu, H. Cheng, J. A. Fan, K.-C. Hwang, J. A. Rogers, Y. Huang, *Acta Mater.* **2013**, *61*, 7816.
- [31] H. C. Ko, M. P. Stoykovich, J. Song, V. Malyarchuk, W. M. Choi, C.-J. Yu, J. B. Geddes Iii, J. Xiao, S. Wang, Y. Huang, *Nature* **2008**, *454*, 748.
- [32] L. Xiao, C. Zhu, W. Xiong, Y. Huang, Z. Yin, *Micromachines* **2018**, *9*, 392.
- [33] S. Jeong, H. Yoon, B. Lee, S. Lee, Y. Hong, *Adv. Mater. Technol.* **2020**, *5*, 2000231.
- [34] O. Oyewole, D. Oyewole, O. Oyelade, S. Adeniji, R. Koech, J. Asare, B. Agyei-Tuffour, W. Soboyejo, *Macromol. Mater. Eng.* **2020**, *305*, 2000369.
- [35] O. K. Oyewole, D. O. Oyewole, M. G. Z. Kana, W. O. Soboyejo, *MRS Adv.* **2016**, *1*, 21.
- [36] J. Liang, L. Li, K. Tong, Z. Ren, W. Hu, X. Niu, Y. Chen, Q. Pei, *ACS Nano* **2014**, *8*, 1590.
- [37] J. Liang, L. Li, X. Niu, Z. Yu, Q. Pei, *Nat. Photonics* **2013**, *7*, 817.
- [38] C. Wang, K. Takei, T. Takahashi, A. Javey, *Chem. Soc. Rev.* **2013**, *42*, 2592.
- [39] J. Li, X. Shan, S. G. R. Bade, T. Geske, Q. Jiang, X. Yang, Z. Yu, *J. Phys. Chem. Lett.* **2016**, *7*, 4059.
- [40] M. G. Helander, Z. B. Wang, J. Qiu, M. T. Greiner, D. P. Puzzo, Z. W. Liu, Z. H. Lu, *Science* **2011**, *332*, 944.
- [41] H. Spreitzer, H. Becker, E. Kluge, W. Kreuder, H. Schenk, R. Demandt, H. Schoo, *Adv. Mater.* **1998**, *10*, 1340.
- [42] O. Kraft, R. Schwaiger, P. Wellner, *Mater. Sci. Eng., A* **2001**, *319–321*, 919.